Taylor-Fourier Multifrequency Approach to Power Quality Monitoring in DC Grids

Riccardo Chiumeo, Christian Laurano, *Member, IEEE* Paolo Attilio Pegoraro, *Senior Member, IEEE*, Antonio Vincenzo Solinas, *Member, IEEE*, Liliana Tenti, Sergio Toscani, *Senior Member, IEEE*, Michele Zanoni *Member, IEEE*

***Abstract*—Direct current (dc) grids and microgrids represent attractive solutions for the integration of renewable energy sources, storage systems and chargers for electric vehicles, all requiring power electronic interface converters. However, there is a severe lack of dedicated measurement tools, both from a scientific and normative point of view. The present paper proposes to extend the concept of wide-area measurements synchronized with respect to an absolute time reference, like the coordinated universal time (UTC) timescale, to dc distribution, which enables observing the state of the grid, tracking dynamics and performing power quality monitoring, in particular measuring the most significant ripple components. In this respect, a class of algorithms, based on a suitably modified Taylor-Fourier Multifrequency (TFM) model, has been developed. Two methods for retrieving the frequency components to be included in the TFM model have been compared: a compressive sensing-based algorithm exploiting the spectral sparsity of the signal, and a new approach using the ESPRIT technique and clustering of spectral components.**

Achieved performance is assessed through numerical simulations that mimic a realistic situation. Results highlight the potentialities of the proposed approaches, that provide highly accurate estimates of the most significant spectral components superimposed to the dc voltage, both under steady-state and dynamic conditions.

***Index Terms*—Direct current, voltage measurement, power quality, synchronized measurement, Phasor Measurement Unit (PMU), ESPRIT, compressive sensing, Taylor-Fourier multifrequency model**

I. Introduction

Distributions systems (DSs) are tasked with enabling a sustainable and reliable achievement of decarbonization and transition towards e-mobility. In this scenario, the diffusion of renewable energy sources (RESs), combined with energy storage systems (ESSs) and electric vehicle charging stations, is expected to grow dramatically. A first consequence is the ubiquitous presence of power electronics converters, as interfaces with the power grid. Moreover, operation becomes highly demanding for the DSs in terms of flexibility and uncertainty of both demand and supply [1].

R. Chiumeo, L. Tenti and M. Zanoni are with TTD, RSE S.p.A., Milano, Italy (email: michele.zanoni@rse-web.it).

C. Laurano and S. Toscani are with Dipartimento di Elettronica, Informazione e Bioingegneria, Politecnico di Milano, Milano, Italy (email: [christian.laurano,sergio.toscani]@polimi.it).

P. A. Pegoraro and A. V. Solinas are with the Department of Electrical and Electronic Engineering of the University of Cagliari, 09123 Cagliari, Italy (email: [paolo.pegoraro,v.solinas]@unica.it).

This work has been financed by the Research Fund for the Italian Electrical System under the Three-Year Research Plan 2022-2024 (DM MITE n. 337, 15.09.2022), in compliance with the Decree of April 16th, 2018.

Direct current (dc) distribution systems and alternate current (ac)/dc microgrids are attractive solutions to effectively integrate RESs, ESSs and electric vehicle charging stations into the current DSs, enhancing power capacity and improving operation flexibility of the system [2]. Some application examples at medium voltage level are the refurbishment of existing ac links to dc [3] or the possibility of weakly meshing the radial ac grid through dc links [4]. Furthermore, Low Voltage dc (LVDC) DSs are established solutions for data centers, transportation and lighting applications. On the other hand, dc and hybrid ac/dc systems demand for specific, advanced control and protection systems [5], [6]. Moreover, these new architectures have to interface with the DSs, which deal with significant operational changes, due to the lower inertia in the transmission grid and higher harmonic content of current and voltage waveforms.

For these reasons, the future trend of DS development asks for more attention to power quality (PQ) aspects: customer requirements are becoming more demanding in terms of continuity and quality of the supply, while dielectric/thermal stresses and resonances have to be, respectively, mitigated and prevented to improve the resilience and reliability of the system [7]. International standards provide the expected PQ levels [8] and PQ measurement requirements [9], with specific attention to harmonics and interharmonics measurements and instrumentation [10], but they refer to conventional ac DSs. Few specific contributions are devoted to PQ in dc and hybrid ac/dc systems, both from a technical and normative point of view, as discussed in [11] and [12]. On the one hand, the importance of investigating the ripple in dc grids signals and understanding its impact on metering is becoming evident [13], on the other hand the normative framework is not consolidated, also from the perspective of definitions and assessment methods.

Some scientific contributions specifically devoted to dc and hybrid ac-dc grids are present in literature. In particular, most of them propose to extend well-known methodologies commonly adopted in ac DSs. Among them, [14] and [15], together with [16], also introduce the metrological aspects of dc power measurements, with specific focus on the presence of spurious contributions. In [17] an index has been proposed to quantify low-frequency (typically up to a few kHz) sinusoidal components superimposed on the mean value. This index consists of the quadratic sum of the respective root mean square (rms) values, thus corresponding to the generalization of the total harmonic distortion to the case of non-periodic

signals. Moreover, another index is defined to globally quantify the ripple in the time domain, i.e., the peak-to-peak amplitude of the sampled signal over a given time window.

In [18] statistical indicators for characterizing PQ parameters in dc microgrids are evaluated in the time domain; in particular, the following quantities are considered: i) the dc component as the mean value of the samples; ii) the median, the peak-to-peak value and the rms value of the ripple; iii) percentiles and asymmetry factors with the aim of quantifying asymmetric disturbances with respect to the mean value. As regards the PQ analysis in the frequency domain, Discrete Fourier Transform (DFT) is computed on each considered signal window.

On the other hand, signal processing techniques widely used in other applications fields have been applied. For example, in [12] frequency domain decompositions as Short Time Fourier Transform (STFT), or time-frequency methods (including wavelets and Empirical Mode Decomposition (EMD)) have been proposed to perform ripple analysis. Then, statistics for the quantification of ripple in the time and frequency domain are reported.

Finally in [19], the most common PQ indexes in dc context are investigated theoretically and experimentally, proposing solutions to mitigate measurement issues that are encountered during practical implementation.

Also international normative committees are moving to fill the gap: the IEC formed the Working Group IEC-TC8-JWG9: "LVDC distribution", which is tasked to carry out a preliminary assessment of PQ requirements for LVDC systems and provide recommendations on voltage level standardization [20]. In this respect, [21] represents a step ahead on the design and validation of reference systems for DC PQ instrumentation testing and their possible employment in a future standardized framework.

However, to the best of our knowledge, dc grids lack specific synchronized measurement instruments. In the same fashion as Phasor Measurement Units (PMUs) in ac systems, they would allow obtaining measurements synchronized with respect to the coordinated universal time (UTC) and thus taking frequent snapshots of the state of the grid, greatly helping its management. Moreover, they could embed advanced PQ monitoring features that enable detecting and quantifying narrowband disturbances in a coordinated way.

In this context, [22] presented for the first time an *ad hoc* algorithm for synchronized dc measurements that allow PQ analysis. The idea of tracking the dynamics of dc voltages and currents along with their ac components (in terms of instantaneous magnitude, phase-angle and frequency) in a frequent and time-tagged way is introduced. The algorithm is based on the Taylor-Fourier Multifrequency (TFM) approach, modeling the signal as a slowly varying dc term superimposed to a sparse set of modulated components. The inherently dynamic representation of the spectral content enables following its time evolution. On the contrary, this is not possible if conventional DFT-based techniques are adopted, which therefore may lead to inaccurate results.

Performance of the TFM method strongly depends on having properly identified and modeled the most significant components, representing the spectral support. In this respect, [22] retrieves the support through Compressive Sensing (CS) [23], using Hann weighting to improve performance [24].

Recently, Estimation of Signal Parameters by Rotational Invariance Technique (ESPRIT) [25] has been employed for detecting and canceling narrowband interferers that may hinder the accuracy of PMU measurements [26]. This has opened the door to ESPRIT application to TFM context.

This article thus, which is the technical extension of [22], proposes a novel support recovery method, based on a tailored version of the ESPRIT algorithm, which cannot be straightforwardly adopted for the purpose. As a matter of fact, ESPRIT has never been applied for the recovery and estimation of modulated components, since it relies on a stationary signal representation. The consequence is that ESPRIT captures a modulated component characterized by a given reference frequency as a set of spectral lines, located in the neighborhood of such reference frequency. In the present paper we propose to restore the match with the dynamic TFM model thanks to an adaptive clustering method. It allows detecting the groups of steady-state terms retrieved by ESPRIT that are likely to be generated by a unique time-varying component.

The proposed TFM-based estimation technique and both CS- and ESPRIT-based support recovery methods have been extensively validated and compared through realistic waveforms, obtained by simulating a simple case study that can be easily implemented by the interested reader. It consists of a parallel 12-pulse rectifier with dc side coupling inductances and filter capacitor, resembling those adopted to supply tramway lines. The dc voltages that result from diverse static and dynamic operating conditions have been processed to obtain synthetic waveforms with known spectra, thus defining references for error calculation. In turn, these waveforms have been used as test signals to assess the accuracy of the developed technique in detecting and estimating disturbances. The results show that both the CS and ESPRIT-clustering based solutions are highly effective. When dynamics in the signals is present, they are able to follow both dc variations and ac components in dc grid signals. The ESPRIT-based technique typically shows a better robustness in these conditions, particularly when noise is present, if the proposed ac components clustering is adopted. Test results prove that the proposed methods are very promising in the detailed and synchronized analysis of dc voltage and current signals.

The rest of the article is organized as follows: Section II introduces TFM models and their peculiarities in the dc context; Section III illustrates the proposed spectral support recovery method; Section IV describes the case study; Section V reports the discussion of the test results while Section VI gives the final remarks and hints on applications and future perspectives.

II. Taylor-Fourier Multifrequency Models for Synchronized Measurements in DC Grids

Let us consider a waveform $x(t)$ from a dc grid, which can be modeled as

$$x(t) = X_0(t) + \sum_{q=1}^{Q} \Re\left\{\bar{X}_q(t) e^{j\omega_q t}\right\} + d(t) \qquad (1)$$

According to (1), the waveform is composed of a prevailing dc term $X_0(t)$, Q significant ac spectral components (namely the ripple) and a wideband disturbance $d(t)$. Each ac or ripple component is defined by a corresponding complex-valued function $\bar{X}_q(t)$ (from here on, overline will always indicate a complex quantity), namely its dynamic phasor referred to the angular frequency ω_q.

Let us suppose that $x(t)$ is sampled with rate f_s (corresponding to the interval T_s) over a rather short window made of $N_w = 2N+1$ samples, centered around the time instant t_r defined in the UTC timescale. If such window does not contain abrupt transients, it is possible to represent the time evolution of $\bar{X}_q(t)$ through a Taylor expansion around t_r, truncated to the order K_q [27]. This enables obtaining a parametric expression for the considered samples, belonging to the class of TFM models. Adopting matrix notation, it results

$$\mathbf{x}(t_r) = \begin{bmatrix} x(t_r - NT_s) \\ \vdots \\ x(t_r) \\ \vdots \\ x(t_r + NT_s) \end{bmatrix} \approx \bar{\mathbf{B}}\bar{\mathbf{p}}(t_r) \tag{2}$$

The model matrix $\bar{\mathbf{B}}$ and the vector of the parameters $\bar{\mathbf{p}}$ are partitioned as

$$\begin{aligned} \bar{\mathbf{B}} &= \begin{bmatrix} \mathbf{B}_0 & \bar{\mathbf{B}}_1 & \underline{\bar{\mathbf{B}}}_1 & \cdots & \bar{\mathbf{B}}_Q & \underline{\bar{\mathbf{B}}}_Q \end{bmatrix} \\ \bar{\mathbf{p}} &= \begin{bmatrix} \mathbf{p}_0^\intercal & \bar{\mathbf{p}}_1^\intercal & \underline{\bar{\mathbf{p}}}_1^\intercal & \cdots & \bar{\mathbf{p}}_Q^\intercal & \underline{\bar{\mathbf{p}}}_Q^\intercal \end{bmatrix}^\intercal \end{aligned} \tag{3}$$

with $\underline{\ }$ denoting the complex conjugate operator. All the parameters depend on t_r, but it will be often omitted for the sake of a lighter notation. In turn,

$$\bar{\mathbf{p}}_q = \begin{bmatrix} \bar{X}_q^{(0)} & \bar{X}_q^{(1)} \cdots \bar{X}_q^{(K_Q)} \end{bmatrix}^\intercal \tag{4}$$

where $\bar{X}_q^{(k)}$ is the kth order derivative of $\bar{X}_q(t)$ in $t = t_r$, with $\bar{X}_q^{(0)} = \bar{X}_q(t_r)$. In order to fully define the model, the generic element in the $(k+1)$th column of $\bar{\mathbf{B}}_q$ for $q \geq 1$ is

$$\bar{\mathbf{b}}_q^k[n] = \frac{(nT_s)^k}{2k!} e^{j\omega_q(t_r + nT_s)} \tag{5}$$

with $-N \leq n \leq N$. The expression of $\mathbf{b}_0^k[n]$ is twice (5), with $q = 0$ and $\omega_0 = 0$. If $\bar{\mathbf{B}}$ has full column rank, an estimate of the model parameters can be obtained with the least squares (LS) approach. It corresponds to minimize a cost function that is the Euclidean norm of the deviation (residual) between the vector of the samples and its reconstruction from the model, namely $\mathbf{r}(t_r) = \mathbf{x}(t_r) - \bar{\mathbf{B}}\bar{\mathbf{p}}(t_r)$. The TFM approach may provide a good, but not exact representation of the samples, which cannot be written as a linear combination between the columns of $\bar{\mathbf{B}}$. This unavoidably leads to estimates that suffer from definitional uncertainty. In order to reduce its impact, it is possible to introduce a diagonal weighting matrix $\mathbf{W} = \mathrm{diag}\,(\mathbf{w})$, so that the resulting cost function $\|\mathbf{r}_w\|$ (with $\mathbf{r}_w = \mathbf{W}\mathbf{r}$) becomes more sensitive to the deviations occurring near t_r. This leads to a new least-squares problem, which is

$$\hat{\bar{\mathbf{p}}}(t_r) = \arg\min_{\bar{\mathbf{p}}} \left\| \bar{\mathbf{B}}_w \bar{\mathbf{p}} - \mathbf{x}_w(t_r) \right\| \tag{6}$$

where $\hat{}$ denotes estimated quantities, $\bar{\mathbf{B}}_w = \mathbf{W}\bar{\mathbf{B}}$ and $\mathbf{x}_w = \mathbf{W}\mathbf{x}$. The solution is $\hat{\bar{\mathbf{p}}} = \bar{\mathbf{H}}_w \mathbf{x}_w$, $\bar{\mathbf{H}}_w = \bar{\mathbf{B}}_w^{\dagger}$[1], thus obtained by projecting $\mathbf{x}_w$ onto the linear space spanned by the weighted TFM model, namely by the set of vectors $\bar{\mathbf{b}}_{w,q}^k = \mathbf{W}\bar{\mathbf{b}}_q^k$. From a different point of view, the rows of $\bar{\mathbf{H}}_w$ contain the coefficients of a bank of FIR filters (known as TFM filters) that enable estimating $\bar{\mathbf{p}}$. Having computed $\hat{\bar{\mathbf{p}}}$, it is possible to extract the dc component associated with the UTC timestamp t_r, estimating the phasors of the other spectral components as well as their frequencies at the same time instant using ($\Im[\cdot]$ is the imaginary part)

$$\hat{f}_q(t_r) = \frac{1}{2\pi} \left(\omega_q + \frac{\Im\left[\hat{\bar{X}}_q^{(1)} \cdot \underline{\hat{\bar{X}}}_q^{(0)} \right]}{\left| \hat{\bar{X}}_q^{(0)} \right|^2} \right) \tag{7}$$

thus requiring $K_q \geq 1$ (see [27] for details).

III. Spectral Support Recovery

The approach presented in Section II assumes having available a fairly accurate TFM model for the observed samples in vector $\mathbf{x}(t_r)$, so that it is possible to build the corresponding matrix $\bar{\mathbf{B}}$ while computing the estimates according to (6). Achieved accuracy is as good as the capability of the TFM model in representing the underlying signal. On the one hand, estimating and tracking the time evolution of a frequency component requires it to be present in the TFM model. On the other hand, if a spectral component of $\mathbf{x}(t_r)$ having relevant magnitude is not included into its TFM representation, it may produce spectral interference, jeopardizing the estimates of the other components. This happens since, in general, the contribution due to such frequency component is not orthogonal to all the columns of $\bar{\mathbf{B}}_w$.

Given the typical dynamics, it is possible to select a reasonable expansion order for capturing the time evolution of the different components. Moreover, it is beneficial to adopt a higher expansion order for the prevailing dc term with respect to the others. However, it is generally not feasible to *a priori* guess what is the set of frequency components to be included in the TFM representation, aside, of course, the dc term. Therefore, a proper technique should be adopted in order to process $\mathbf{x}$ for identifying the set $\mathbb{S}$ of the most significant narrowband components (which is the spectral support of the observed samples) resulting in a retrieved set $\hat{\mathbb{S}}$. In this respect, the adopted TFM matrix is the outcome of an estimation, thus it will be indicated with $\hat{\bar{\mathbf{B}}}$, being $\hat{\bar{\mathbf{B}}}_w$ its weighted counterpart. The most trivial approach to obtain $\hat{\mathbb{S}}$ is adopting a DFT-based method and searching for the strongest spectral lines. However, a severe limitation comes from the inherent frequency resolution, which is $\Delta\omega = 2\pi/(N_w T_s)$. In fact, a window length which is small enough to track the time evolution of the components corresponds to a coarse frequency resolution. In turn, this makes that the estimates suffer from significant definitional uncertainty. Therefore, more advanced spectral support recovery methods must be considered.

[1] † denotes the Moore-Penrose inverse.

A. Compressive Sensing-Based Approach

In many practical situations, the observed segment of signal contains a small number S of spectral components that emerge from wideband noise and worth to be included in the TFM model. Let us suppose that $S \leq Q_{\max} \ll N_w$. This means that, once having selected a proper TFM basis, the vector of the samples is well approximated through a sparse representation. Retrieving the spectral support means defining this basis, thus finding the set of at most $Q_{\max}$ frequency components that, when included in the TFM model, enable minimizing the norm of $\mathbf{r}_w$ resulting from the LS solution.

Recovering the support thus requires solving a very computationally-intensive optimization problem. An approximate solution can be achieved through the CS Weighted TFM (CS-WTFM) approach presented in [24], which can be favorably adapted to dc applications. Let us firstly introduce a grid of super-resolved angular frequency values, i.e., whose spacing is $\delta\omega < \Delta\omega$. The generic hth frequency value of the grid is one of the possible elements of the recovered support $\hat{\mathbb{S}}$ and is matched with a corresponding column vector $\bar{\mathbf{d}}_{h,w}$ (called atom) containing N_w samples of the complex exponential with rotational speed $h\delta\omega$ multiplied by $\mathbf{W}$. The set of the atoms forms the dictionary.

The support is retrieved through a greedy algorithm, consisting of at most $Q_{\max}$ iterations. Each step is aimed at finding what is the frequency component among the candidates that, when included into the model, results in the largest decrease of the cost function. Before the generic ith iteration, we have a TFM model defined by matrix $\hat{\bar{\mathbf{B}}}^{[i-1]}$, including $i-1$ spectral components other than the dc; let us call $\mathbf{r}_w^{[i-1]}$ the obtained residual and $\hat{\mathbb{S}}^{[i-1]}$ the corresponding set of frequencies so far identified. During the ith step, all the atoms corresponding to the frequency candidates are projected on $\mathbf{r}_w^{[i-1]}$, which means computing the scalar product. The angular frequency value (i.e., the value $h\delta\omega$) resulting in the largest projection is then included in the support, thus defining $\hat{\mathbb{S}}^{[i]}$. The updated TFM matrix $\hat{\bar{\mathbf{B}}}^{[i]}$ is obtained by appending to $\hat{\bar{\mathbf{B}}}^{[i-1]}$ the two conjugate submatrices associated with the new component. Equation (6) enables computing the parameters of the augmented TFM model, and in turn also the new residual $\mathbf{r}_w^{[i]}$. The iterative procedure stops if i exceeds $Q_{\max}$, or if the norm of $\mathbf{r}_w^{[i]}$ is below a predetermined threshold.

The overall computational burden depends on $\delta\omega$, N_w and $Q_{\max}$, but in [24] the possibility to easily get a high measurement rate is proven.

B. ESPRIT and Clustering-Based Approach

The ESPRIT method [25] is a highly effective technique to identify the frequency components in a multisinuosidal signal that arise from wideband noise. Therefore, with proper modifications, it appears suitable for obtaining $\hat{\mathbb{S}}$. Considering $-N \leq n \leq N$, the following model of the observed samples is adopted

$$x(t_r + nT_s) = s(t_r + nT_s) + u(t_r + nT_s)$$
$$s(t_r + nT_s) = \sum_{p=0}^{P} \left[\bar{Z}_p(t_r) e^{j\gamma_p nT_s} + \underline{Z}_p(t_r) e^{-j\gamma_p nT_s}\right] \quad (8)$$

Samples are thus decomposed into the useful signal $s(t_r+nT_s)$ and a superimposed zero-mean noise contribution $u(t_r+nT_s)$ having variance σ_u^2. In turn, signal has been written as a linear combination of $P+1$ pairs of counter-rotating exponentials, having angular frequencies $\{\gamma_p\}_{p\in\{0,\dots,P\}}$, while the corresponding amplitudes and initial phases are set by $\{\bar{Z}_p(t_r)\}_{p\in\{0,\dots,P\}}$. It is worth noting that both (8) and (2) can be adopted as alternative representations for the samples of the observed segment of waveform, having an expression in the form (1). The TFM model (2) relies on dynamic spectral components, which in general may have time-varying magnitude and frequency. Instead, (8) decomposes the signal in stationary components, having constant magnitude and frequency in the considered interval. The consequence is that the qth modulated component appearing in (1) may induce several rotating exponential terms in (8), thus P could be considerably larger than Q.

The first step of the ESPRIT method is rearranging the observed samples in $L = N_w - M + 1$ overlapped records having length $M > 2(P+1)$. The generic lth record, $l \in \{1,\dots,L\}$, is

$$\mathbf{x}^{[l]}(t_r) = \begin{bmatrix} x(t_r + (l-1-N)T_s) \\ \vdots \\ x(t_r + (l+M-2-N)T_s) \end{bmatrix} \quad (9)$$

Reminding (8), we can separate the signal and noise contributions, thus $\mathbf{x}^{[l]} = \mathbf{s}^{[l]} + \mathbf{u}$, where $\mathbf{u}$ is a random vector having independent entries, characterized by the same variance σ_u^2. From here on, dependency on t_r will be omitted for the sake of brevity.

Using (8), the signal contribution to the lth record can be expressed as

$$\mathbf{s}^{[l]} = \bar{\mathbf{E}}\bar{\mathbf{\Phi}}^{l-1}\bar{\mathbf{z}} \quad (10)$$

having introduced the rotation matrix

$$\bar{\mathbf{\Phi}} = \mathrm{diag}\left(\begin{bmatrix} e^{j\gamma_0 T_s} & e^{-j\gamma_0 T_s} & \dots & e^{-j\gamma_P T_s}\end{bmatrix}\right) \quad (11)$$

while

$$\bar{\mathbf{z}} = \begin{bmatrix}\bar{Z}_0 & \underline{Z}_0 & \dots & \underline{Z}_P\end{bmatrix}^{\mathsf{T}} \quad (12)$$

$$\bar{\mathbf{E}} = \begin{bmatrix}\bar{\mathbf{e}}_0 & \underline{\mathbf{e}}_0 & \dots & \underline{\mathbf{e}}_P\end{bmatrix} \quad (13)$$

In turn, $\bar{\mathbf{e}}_p$ is a column vector containing M samples of a rotating exponential with angular frequency γ_p (with time instant index $n = -N,\dots,-N+M-1$).

Let us introduce $\bar{\mathbf{E}}_{M-1}$ as the matrix made of the first $M-1$ rows of $\bar{\mathbf{E}}$. We can define

$$\bar{\mathbf{V}}_{\mathrm{L}} = \bar{\mathbf{E}}_{M-1}\bar{\mathbf{\Phi}}^{l-1} \qquad \bar{\mathbf{V}}_{\mathrm{R}} = \bar{\mathbf{E}}_{M-1}\bar{\mathbf{\Phi}}^{l} \quad (14)$$

Reminding (10) and the structure of $\bar{\mathbf{E}}$, the columns of the matrices $\bar{\mathbf{V}}_{\mathrm{L}}$ and $\bar{\mathbf{V}}_{\mathrm{R}}$ are basis for the the first and last $M-1$ rows of $\mathbf{s}^{[l]}$, respectively. Moreover, according to (14), they are related through the rotation matrix.

Now, let us consider the autocorrelation matrix of the data records, defined as

$$\mathbf{R} = \mathbb{E}\left[\mathbf{x}^{[l]}\left(\mathbf{x}^{[l]}\right)^{\intercal}\right] \tag{15}$$

where $\mathbb{E}(\cdot)$ is the expectation operator. Let us define vector $\boldsymbol{\xi}$ containing the singular values of $\mathbf{R}$, sorted in decreasing order. It is possible to demonstrate that the first $2(P+1)$ elements of $\boldsymbol{\xi}$ capture energy from both signal and noise, thus they are larger than the others, which are in turn purely related to noise and all equal to σ_u^2 [28]. Matrix $\mathbf{U}$ containing the corresponding eigenvectors is partitioned as

$$\mathbf{U} = \begin{bmatrix}\mathbf{U}_s & \mathbf{U}_u\end{bmatrix} \tag{16}$$

The columns of $\mathbf{U}_s$ span a $2(P+1)$-dimensional subspace called signal subspace[2], while those of $\mathbf{U}_u$ generate a $[M-2(P+1)]$-dimensional subspace, known as noise subspace. In the presence of a reasonably good signal-to-noise ratio (SNR), $\mathbf{U}_s$ provides a basis for $\mathbf{s}^{[l]}$. Therefore, if $\mathbf{U}_{\mathrm{L}}$ and $\mathbf{U}_{\mathrm{R}}$ are the first and last $M-1$ rows of $\mathbf{U}_s$, it exists a full-rank transformation matrix $\bar{\mathbf{T}}$ so that

$$\bar{\mathbf{V}}_{\mathrm{L}} = \mathbf{U}_{\mathrm{L}}\bar{\mathbf{T}} \qquad \bar{\mathbf{V}}_{\mathrm{R}} = \mathbf{U}_{\mathrm{R}}\bar{\mathbf{T}} \tag{17}$$

From (14) and (17), we obtain

$$\mathbf{U}_{\mathrm{L}}\bar{\boldsymbol{\Psi}} = \mathbf{U}_{\mathrm{R}} \qquad \bar{\boldsymbol{\Psi}} = \bar{\mathbf{T}}\bar{\boldsymbol{\Phi}}\bar{\mathbf{T}}^{-1} \tag{18}$$

Equation (18) provides the eigendecomposition of $\bar{\boldsymbol{\Psi}}$, whose eigenvalues are in the rotation matrix $\bar{\boldsymbol{\Phi}}$. This property enables retrieving the frequencies $\{\gamma_p\}_{p\in\{0,\dots,P\}}$ of the components that, according to (11), are the positive arguments of the eigenvalues of $\bar{\boldsymbol{\Psi}}$ divided by T_s. From (18), a LS estimate of $\bar{\boldsymbol{\Psi}}$ is obtained as

$$\hat{\bar{\boldsymbol{\Psi}}} = \mathbf{U}_{\mathrm{L}}^{\dagger}\mathbf{U}_{\mathrm{R}} \tag{19}$$

However, the autocorrelation matrix $\mathbf{R}$, thus $\mathbf{U}_{\mathrm{L}}$ and $\mathbf{U}_{\mathrm{R}}$, are not known: they must be estimated from the samples. For this purpose, let us organize the L records defined by (9) in a $M \times L$ Hankel matrix

$$\mathbf{X} = \begin{bmatrix}\mathbf{x}^{[1]} & \cdots & \mathbf{x}^{[L]}\end{bmatrix} \tag{20}$$

It is worth noting that $\hat{\mathbf{R}} = \mathbf{X}\mathbf{X}^{\intercal}/L$ represents an unbiased estimate of $\mathbf{R}$. In turn, it can be easily proven that both the singular values and the eigenvectors of $\hat{\mathbf{R}}$ can be computed from $\mathbf{X}$; estimates of $\boldsymbol{\xi}$ and $\mathbf{U}_s$ are thus obtained.

The ESPRIT technique requires separating the signal subspace, which means obtaining its size $2(P+1)$. In general, it is not known in advance, but it could be gathered from the estimated singular values in $\hat{\boldsymbol{\xi}}$. The adopted method shall be robust enough, since $\hat{\boldsymbol{\xi}}$ represents an estimate (which is as good as L is large) and (8) is an idealization. A possibility is choosing $P_{\max}$ so that $P \leq P_{\max}$ and averaging the last $M-2(P_{\max}+1)$ elements of $\hat{\boldsymbol{\xi}}$: this provides a better evaluation $\hat{\sigma}_u^2$ of noise variance with respect to trusting a sole singular value. Then, an estimate of P is obtained by counting the number of elements in $\hat{\boldsymbol{\xi}}$ that exceed $G\hat{\sigma}_u^2$, with G being a user-defined value.

[2]Note that also noise produces contributions belonging to the signal subspace.

In the present article, ESPRIT is applied to retrieve the spectral support of the measured signal, defined by vector $\hat{\boldsymbol{\gamma}}$ containing frequency estimates. However, reminding (8), this set of frequencies is tied to a static model of the components, which are assumed to be constant in amplitude and frequency over the N_w-sample window. Therefore, in order to be consistent, this implies adopting a TFM model (2) with zeroth order expansion. Such a straightforward application of ESPRIT enables heavily mitigating the spectral interference affecting the estimates obtained from (6), once having assumed that the measured component is perfectly steady-state. However, having moved towards a stationary frequency-domain representation of the signal, it would no longer be possible to properly track the time evolution of such component, thus neutralizing the main advantage of the TFM-based approach.

The proposed idea to overcome this issue, thus effectively combining ESPRIT-based support recovery with a dynamic TFM signal model, is reminding that each term in (1) produces, when considering the stationary representation (8), a cluster of sideband components around a given frequency ω_c. Therefore, one may identify the cluster of frequencies in $\hat{\boldsymbol{\gamma}}$ having bandwidth below a predetermined threshold, which would lead to a single component in the TFM model, represented through a Taylor expansion of the phasor centered on ω_c.

After sorting in ascending order the found angular frequencies in $\hat{\boldsymbol{\gamma}} = [\cdots\hat{\gamma}_p\cdots]^{\intercal}$ with $p \in \{0,\dots,P\}$, the clustering process starts from the lowest frequency, i.e. from the dc. All values $\hat{\gamma}_p \leq \Delta\omega_c$, with $\Delta\omega_c$ the clustering parameter, are considered in the dc cluster. The remaining frequencies in $\hat{\boldsymbol{\gamma}}$ are then analyzed in increasing order. If a frequency value is separated by at most $\Delta\omega_c$ from the previous one, it is clustered with it. The process is iterative and the ac cluster is closed when the next frequency is farther than $\Delta\omega_c$ from the highest frequency or $2\Delta\omega_c$ from the lowest frequency already present in the cluster. If a cluster includes only one frequency value, it corresponds to an isolated monochromatic component, whereas, if it is composed of more than a single frequency, it can be considered as a proper cluster associated with frequency 0 rad/s for the dc cluster, or with ω_c obtained by averaging all the frequencies of the clustered components when it represents a ripple component.

It is worth noting that some components in (1) may not undergo significant modulation, therefore they can be properly modeled in (2) with just a zeroth, or at most a first order Taylor-Fourier expansion for increasing the robustness of the estimates with respect to inaccuracies in the retrieved spectral support. On the other hand, an unnecessarily high expansion order leads to larger lobes in the corresponding filter frequency response. This increases the sensitivity of each estimate with respect to wideband noise and to the remaining disturbances. Here it is thus proposed to improve overall performance by adopting an expansion order greater than one only when a cluster of components is detected.

IV. Case Study

The target is assessing the achieved performance in measuring the dc and the most significant ripple components

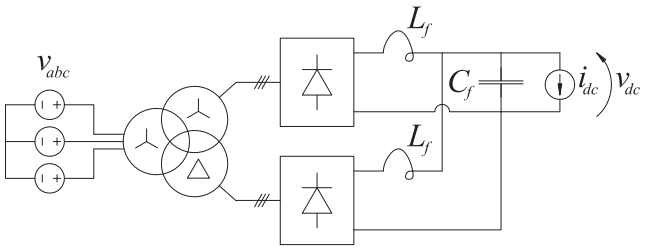

Fig. 1: Diagram of the considered 12-pulse diode rectifier.

through the TFM approach, while comparing the CS and ESPRIT-clustering support recovery techniques. Such analysis should be carried out considering typical waveforms found in dc grids. Due to the lack of information in this regard, we have chosen to obtain test waveforms by considering a simple case study, which is easily reproducible by the interested reader. It is based on a 12-pulse diode rectifier, resembling those typically adopted to supply tramway contact lines; its schematic diagram is shown in Fig. 1.

The core-type, three-winding transformer has $2.5\,\text{MVA}$ rated power and $50\,\text{Hz}$ nominal frequency. Rated voltages, connections, series resistances and leakage inductances are listed in Table I. Magnetizing resistance and inductance are $893\,\text{p.u.}$ (base primary impedance $211.6\,\Omega$) and $346\,\text{p.u.}$, respectively, while the total inductance of the zero-sequence flux path is $2\,\text{p.u.}$

The transformer is supplied by a three-phase, $50\,\text{Hz}$ grid with infinite short circuit power. Each of the two secondary windings, having $30°$ mutual phase shift, feeds a three-phase bridge rectifier. Inductors $L_f = 3\,\text{mH}$ allow the dc-side connection between the two bridges and, together with capacitor $C_f = 94\,\mu\text{F}$, provide filtering aimed at further reducing the ripple affecting v_{dc}. Load is modeled as an ideal current source drawing i_{dc} from the rectifier. In order to stress the considered estimation algorithms, a more complex dc side spectrum can be obtained by changing the ac supply conditions with respect to the nominal three-phase symmetric sinusoidal voltage.

The previously described rectifier model has been implemented in Simulink/Simscape environment. Voltage v_{dc} has been observed with $1\,\text{MHz}$ rate under different operating conditions, both in terms of load and ac voltage supply. Its spectrum has been estimated through a DFT performed on a $1\,\text{s}$ time window. For each considered condition, the most significant spectral components have been identified and properly processed in order to build a counterpart of v_{dc} closely resembling that computed from the simulation. In this way, the synthesized waveform has perfectly known spectral content, which acts as a reference for the estimation error computation of each considered component in each instant. Indeed, in this way, it is possible to define the deviations between used ground-truth values and corresponding estimates, thus quantifying achieved performance in a metrologically-sound way.

TABLE I: Transformer Series Parameters

Parameter	Winding 1	Winding 2	Winding 3
V_n [kV]	23	0.456	0.456
Connection	Y0	Y0	D11
R_s [p.u.]	$6.3 \cdot 10^{-3}$	$1.2 \cdot 10^{-2}$	$1.2 \cdot 10^{-2}$
L_s [p.u.]	0.18	$6.8 \cdot 10^{-3}$	$1.8 \cdot 10^{-2}$

Except when otherwise stated and explicitly recalled, all the tests in Section V have been performed using the above described procedure to synthesize the test waveforms. When a test is repeated changing a parameter, the whole process is executed again to find the new spectrum and generate realistic signals accordingly.

V. Tests and Results

The presented algorithms have been compared using simulated signals defined starting from the case study in Section IV. In particular, the proposed ESPRIT-clustering-based TFM algorithm (EC-WTFM) is compared with the CS-WTFM, whose spectral support search is described in Section III-A, and with a straightforward ESPRIT application to TFM model identification (ESPRIT-WTFM from here on). The aim is to investigate, by using the same LS-based TFM parameter estimation, what is the impact of different spectral support estimation algorithms on dc and ac measurements.

The tests rely thus on dc+ac signals and are partially inspired by those of current PMU standard [29], because we are actually monitoring also dynamic phasors at different ac frequencies. The focus here is mainly on realistic test scenarios and on the measurement algorithm, whereas other sources of errors (such as those introduced by the adopted instrument transformer) might appear in a real implementation.

In all the tests and for all the algorithms, the synchronized estimates of the dc voltage and the synchronized measurements of phasor and frequency of each ripple component are computed with a fixed reporting rate (RR) and compared with the reference values (of magnitude, phase-angle and instantaneous frequency) available in each measurement instant thanks to the procedure described in Section IV. Plain estimation error is used for the assessment of dc component measurement. As for ripple components, the percent Total Vector Error (TVE), i.e., the relative vector error, is used to quantify the accuracy for synchronized phasors estimates, while the Frequency Error (FE) is the performance index for component localization. The discussion on the estimation accuracy in the following sections will rely on these errors computed for each test.

A. Steady-State Conditions

The first test set corresponds to steady-state conditions of the ac supply voltage v_{abc} (sinusoidal and symmetric at rated frequency) and to constant load (i_{dc} is constant and equal to its rated value during all the tests). The test duration is $5\,\text{s}$ for all the considered cases unless otherwise specified. An example of a simulated v_{dc} spectrum (computed with $1\,\text{Hz}$ resolution) is reported in Fig. 2 (base test case). It reveals the presence of three terms: the dc and 2 ac components located at $600\,\text{Hz}$ and $1200\,\text{Hz}$, i.e., the fundamental and second harmonic of the theoretical ripple of a 12-pulse rectifier. Such spectral content can change depending on the test conditions. In particular,

several signals have been simulated adding non-idealities to the ac supply (see Section IV for details). Harmonic and interharmonic interferers have been introduced, leading to richer spectra than that of Fig. 2 (see for instance Fig. 5 below and the corresponding discussion), since the rectifier yields combinations of the input frequency components beside those already present under nominal conditions.

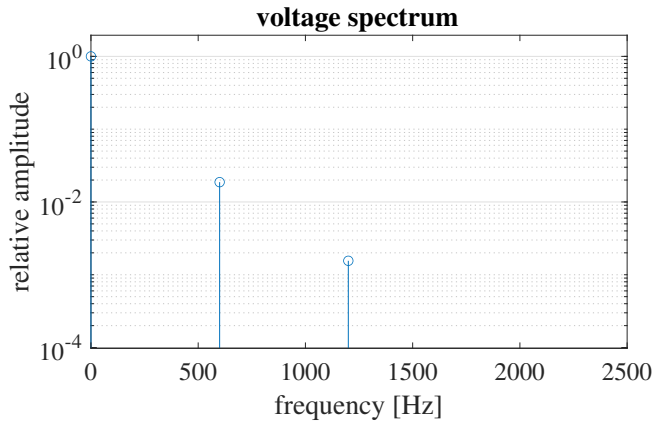

Fig. 2: Nominal steady-state test condition – dc-side voltage spectrum (amplitudes are relative to the dc component).

All three methods have been implemented using a sampling rate of 5 kHz and a RR of 100 measurements per second (half nominal ac cycle shift between consecutive measurements) has been used for analysis purposes. In this paper, we limit the investigation to the low frequency region of the spectrum, but, in principle, depending on the available hardware and on the computation power, the same methods could be employed to explore other ranges and higher frequencies. An analysis window of approximately 200 ms ($N_w = 10 \cdot 100 + 1$, where 10 is the number of observed nominal cycles, 100 the number of samples per period and 1 is added to obtain an odd window length) has been chosen to mimic the behavior of PQ meters according to [9] and samples are weighted by Hann window. Also in this regard, the proposed configuration is only an example, close to what is nowadays discussed in the scientific community, but there are no limits in principle in adapting it to other monitoring targets or applications. The best spectral support is sought having included *a priori* the zero-frequency component; expansion order 4 is adopted for dc, while order 3 is used for ac components in CS-WTFM and in EC-WTFM when a cluster is identified. When EC-WTFM finds monochromatic components or in ESPRIT-WTFM (which assumes isolated and independent frequency components) order 1 is used to address frequency deviations from the initial spectral support estimation. The CS-WTFM implementation adopts $\delta\omega = 4\pi$ rad/s for the dictionary frequency grid (thus corresponding to 2 Hz) and, to avoid any possibly unfair settings, is assumed to know the maximum cardinality of the TFM support (thus setting $Q_{\max} = |\mathbb{S}|$). A threshold value $10^{-3} \cdot \|\mathbf{x}_w\|$ is chosen as stop condition for the residual norm (see Section III-B). EC-WTFM assumes $\Delta\omega_c = 18\pi$ rad/s.

In steady-state and nominal conditions, the underlying signal models of all methods almost perfectly match the actual spectral content, leading to negligible measurement errors for both dc and ac components, as in [22]. For CS-WTFM, this is a consequence of the fact that components appearing in Fig. 2 fall exactly on dictionary frequency grid. If additive white uniform noise is superimposed on the signals, errors mainly depend on the equivalent noise bandwidths of the adopted TFM filters.

Since all the methods are based on WTFM models, hence identical results would be obtained if the same components were identified and represented with the same expansion orders. However, slight differences in spectral support computation emerge between CS- and ESPRIT-based algorithms, as a result of their inherently different approaches. Furthermore, even if all three methods locate three components with negligible frequency deviations, they lead to different TFM models. In fact, while CS-WTFM relies on a third-order expansion of the phasors, ESPRIT-WTFM adopts first order expansions and the same is chosen by EC-WTFM, since, in this case, only isolated frequencies are found. This difference in the underlying models is reflected in the equivalent noise bandwidth. Indeed ESPRIT-based solutions lead to different TFM filters and, in particular, narrower bandwidths as far as ac components are concerned, thus resulting in lower noise infiltration. This is exactly the outcome of the tests with additive noise at 80 dB SNR (which is always kept in all the following tests). Dc errors are always lower than $1 \cdot 10^{-3}$ %, thus negligible for practical applications, but the dc component rms error achieved by CS-WTFM is almost double with respect to the others.

Focusing on the two ac components (600 Hz and 1200 Hz), the maximum TVEs are below 0.09 % and 0.9 % for the ESPRIT-based methods, while that of CS-WTFM is almost 40 % higher. A full analysis of noise impact on WTFM is beyond the scope of the paper; however, it can be reduced through different strategies, such as selecting higher sampling rate, a longer window or by adding a pre-filtering input stage.

Similar results have been found when dealing with 1 % voltage unbalance (1 % superimposed negative sequence component) in the ac supply. The main difference is in the dc spectrum, where 100 Hz and 500 Hz spectral lines, larger than that at 1200 Hz, appear. Once again, all the methods almost perfectly estimate the dc and ac components in the absence of noise. In fact, the actual spectral components belong to the frequency grid defining the dictionary used by the CS-WTFM, which results in exact spectral support identification, but both ESPRIT-WTFM and EC-WTFM are again able to estimate such frequencies with negligible errors. When noise at 80 dB SNR is considered, results similar to those of the balanced supply case are obtained and the same considerations apply. All the following tests have been performed considering symmetric ac voltage.

In order to test the robustness with respect to off-nominal frequency conditions, the base test case has been repeated several times changing only the ac supply frequency $f_{0,\text{ac}}$ from 48 Hz to 52 Hz (step 100 mHz), which represents the steady-state off-nominal frequency test interval for P-class compliance prescribed by the PMU standard; the two ac components in dc spectrum move accordingly. Differently

from the other tests, this test is performed just re-synthesizing the waveform corresponding to the spectrum shown in Fig. 2 with rescaled frequency axis according to every off-nominal condition and adding noise. The dc measurement error is below $10^{-3}\,\%$, thus still negligible for all the algorithms and not significantly affected by $f_{0,\mathrm{ac}}$.

Figure 3 quantifies, in terms of rms TVE, the achieved accuracy in estimating the first significant ac component in the dc-side voltage (its frequency is 12 times $f_{0,\mathrm{ac}}$) as a function of the ac supply fundamental frequency. Under off-nominal frequency conditions, the spectral support can easily include frequencies that are not part of the dictionary set, since not only even integer frequency values are involved. Indeed, when $f_{0,\mathrm{ac}} \notin \{48, 48.5, 49, 49.5, 50, 50.5, 51, 51.5, 52\}$ Hz, the ac components of the ripple fall off the dictionary grid. This means that in many cases CS-WTFM cannot reach the actual support, being it limited by the 2 Hz frequency resolution of the adopted dictionary. However, it finds always the closest frequency in the dictionary for every component (offset between actual and retrieved component below 1 Hz) and its rms FEs are always lower than 2.4 mHz and 28.3 mHz for the first and second ac components, respectively. This confirms that, thanks to the 3rd order expansion, WTFM is able to cope also with significant deviations between the frequencies in the support and the actual ones. On the other hand, ESPRIT-WTFM and EC-WTFM methods find a more accurate initial support (maximum frequency deviation 2.1 mHz and 23.9 mHz for first and second ac component, respectively) thus improving the TFM model definition and the consequent estimation (the rms FEs across all the off-nominal tests are below 1.2 mHz and 13.3 mHz).

Having considered steady-state test conditions, ESPRIT-based algorithms with or without clustering compute identical estimates, resulting in the same TVE values as noticeable from Fig. 3. Furthermore, as discussed above, lower expansion orders lead to TFM filters that reduce the noise impact, thus explaining why Fig. 3 shows differences among CS and ESPRIT-based algorithms. In any case, as from Fig. 3, error values are negligible from a practical point of view, and they confirm that all the algorithms are capable of adapting every filter center frequency, since no significant degradation can be found as $f_{0,\mathrm{ac}}$ deviates from its rated value. Non-negligible (albeit rather small) errors are achieved for the second frequency component (i.e., that at frequency $24 \cdot f_{0,\mathrm{ac}}$) as shown in Fig. 4 that reports, like Fig. 3, the rms TVE as a function of $f_{0,\mathrm{ac}}$. TVE values are over ten times larger than before, but the behaviors of the algorithms are identical to those observed in Fig. 3 and similar considerations can be drawn.

It is interesting to test the algorithms also in the presence of additional components. In particular, a positive sequence interferer at a frequency $f_{\mathrm{ih,ac}}$ not multiple of $f_{0,\mathrm{ac}}$ (thus indicated as interharmonic, ih, in what follows) has been superimposed on the base test case, i.e., on the ac supply voltage when no other disturbances except noise are present. Its rms magnitude is $1\,\%$ of the $f_{0,\mathrm{ac}}$ component and its frequency varies (with 1 Hz step) in the ranges $10 \div 25$ Hz and $75 \div 95$ Hz, like in the out-of-band interference test prescribed

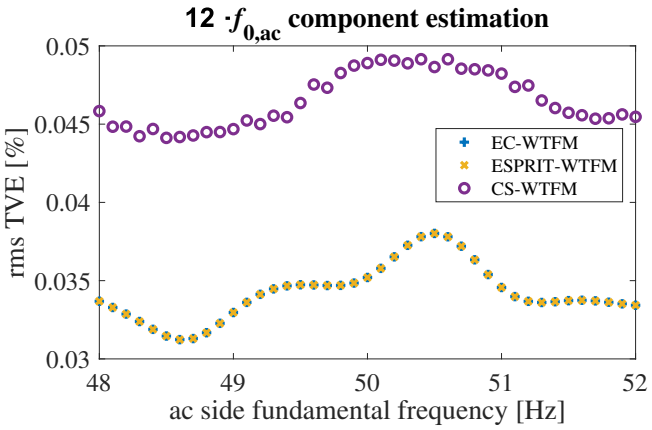

Fig. 3: Off-nominal frequency test (SNR 80 dB) – rms TVE of the $12 \cdot f_{0,\mathrm{ac}}$ component estimation.

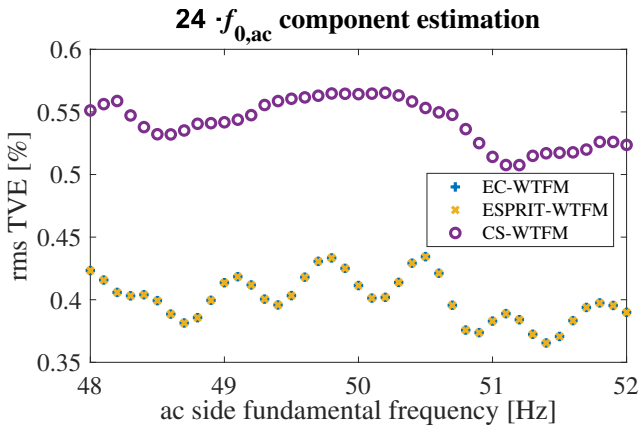

Fig. 4: Off-nominal frequency test (SNR 80 dB) – rms TVE of the $24 \cdot f_{0,\mathrm{ac}}$ component estimation.

by the PMU standard [29]. An example of the dc voltage waveform, simulated with $f_{\mathrm{ih,ac}} = 19$ Hz, is reported in Fig. 5a, while the relative amplitude of its spectrum with respect to dc component is shown in Fig. 5b. Two oscillations superimposed to the dc voltage are clearly visible: the faster one corresponds to a 600 Hz frequency with an amplitude of about $1.8\,\%$; the second and slower one corresponds to a component having $0.8\,\%$ magnitude, located at a frequency $f_{\mathrm{ih,dc}} = 31$ Hz, i.e., the absolute difference between the nominal ac system frequency and the frequency of the injected interharmonic, thus resulting from inter-modulation produced by the rectifier. There are also other weaker components at 1200 Hz and close to the 600 Hz component (± 31 Hz sideband components).

The rms error of the dc estimate is still negligible and there is no significant influence from the interharmonic, since the lowpass filter that enables extracting the dc has similar characteristics for all the methods. The aforementioned considerations still hold also in this case, with ESPRIT-based algorithms achieving almost halved errors. As expected, EC-WTFM and ESPRIT-WTFM rely on the same TFM model, since the considered signal is made only of stationary components.

Higher errors are obtained when looking at ac components

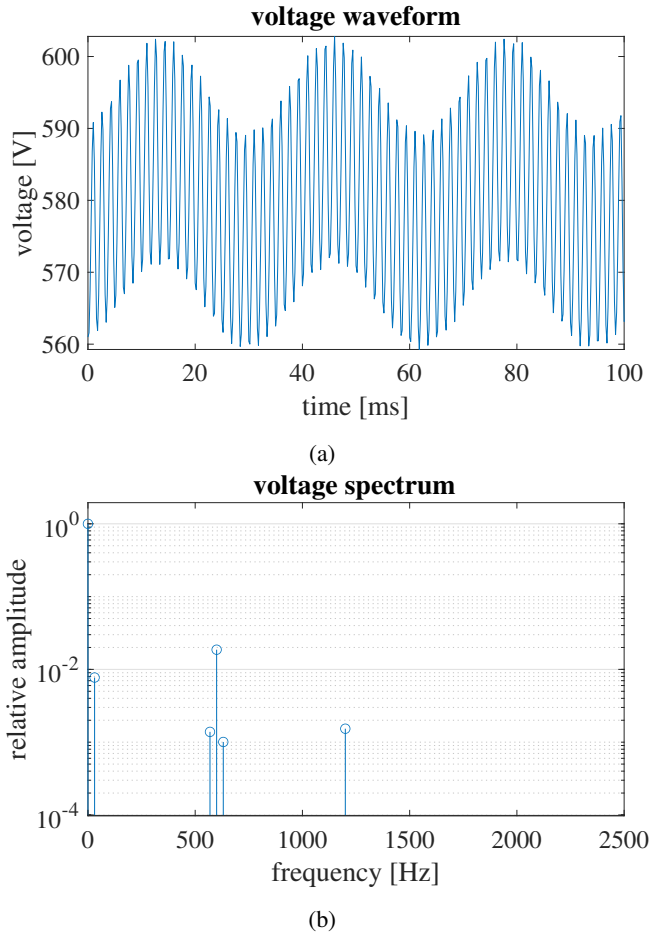

Fig. 5: Interharmonic test with $f_{\text{ih,ac}} = 19\,\text{Hz}$ – (a) waveform, (b) spectrum (amplitudes are relative to the dc component).

estimation, as summarized in terms of rms TVE by Figs. 6 and 7, which report the rms TVE values for 600 Hz component and $f_{\text{ih,dc}}$ component, respectively. Nevertheless, the same aforementioned considerations still apply. The two figures exhibit two horizontal axes to make the dc side effect of the interharmonic injection easier to interpret. The bottom axis indicates the interharmonic frequency $f_{\text{ih,ac}}$ of the disturbance superimposed on the ac side supply voltage (see Fig. 1), while the top axis reports the frequency $f_{\text{ih,dc}}$ of the corresponding dc side disturbance downstream the rectifier. The latter is indeed the resulting frequency of the slowest additional component that can be found, in this conditions, in the dc ripple, and it is reported to make more evident its distance with respect to dc. Such frequency results from the interaction between $f_{0,\text{ac}}$ or its multiples with $f_{\text{ih,ac}}$, because of the nonlinear behavior of the rectifier. Depending on the tests, different significant components can appear in the dc spectrum, but that closest to dc gives directly some hints on the interharmonic disturbance transformation. It is important to stress that Fig. 6 investigates only the estimation accuracy of the 600 Hz component when varying the frequency of the interharmonic disturbance. On the contrary, Fig. 7 focuses on the estimation of the aforementioned slowest interharmonic ac component that appears in the dc spectrum. Each point of the graph corresponds to

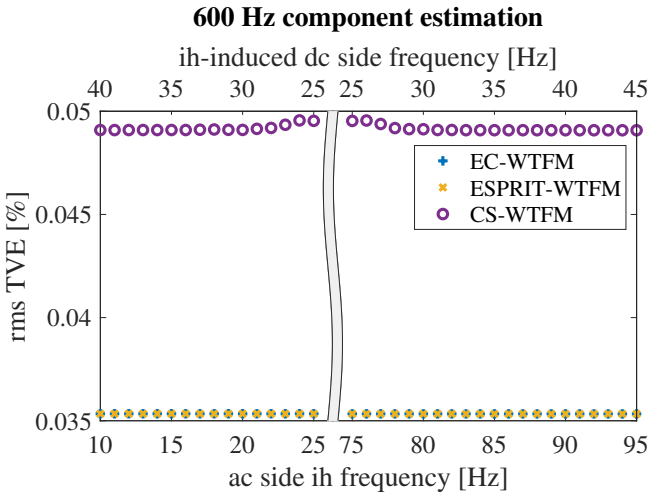

Fig. 6: Interharmonic test (SNR 80 dB) – rms TVE of the 600 Hz component estimation.

the rms TVE of the estimated synchronized phasor for such disturbance, when a specific interharmonic having frequency $f_{\text{ih,ac}}$ (readable on the bottom axis) is superimposed. The new component changes its position in the spectrum of the dc waveform according to the top x-axis.

It is important to notice that, in such tests, the interharmonic component does not always fall on the dictionary grid, since $f_{\text{ih,ac}}$ is swept with a 1 Hz step, while grid resolution is 2 Hz. However, CS-WTFM always gets the best possible support from the dictionary. Results confirm that the impact of dictionary resolution is negligible for interharmonic estimation (no bumps in the TVE trend are visible on odd frequencies). Comparing Fig. 7 with Fig. 6, the higher the rms magnitude of the component to be estimated, the better are the results (lower TVE), but the difference between CS-WTFM and ESPRIT-based algorithms is evident and mainly due to noise infiltration, like in the previous cases. The trend of rms TVE, while highlighting a slight decrease as the measured component becomes closer to 25 Hz, still shows the remarkable performance of the three methods.

B. Dynamic Conditions

More interesting, in terms of differences among the algorithms, are the results obtained under dynamic conditions, such as slow variations in the ac supply. In particular, sinusoidal amplitude modulation (AM) and phase modulation (PM) conditions have been simulated through the model presented in Section IV. In what follows, only the first test type is discussed, since it is the most interesting and demanding for the scenario at hand. AM at ac side induces AM also in the dc voltage, but the ripple components appearing in such voltage undergo a more complex evolution. Indeed, pairs of lateral neighbor components at a distance equal to (or multiple of) the modulation frequency can also appear for dc-side ac components. Such components represent slow variations, thus spectrum thresholding alone is no longer a valid approach to synthesize the reference quantities from the simulation results. For this reason, in addition to the amplitude modulated dc,

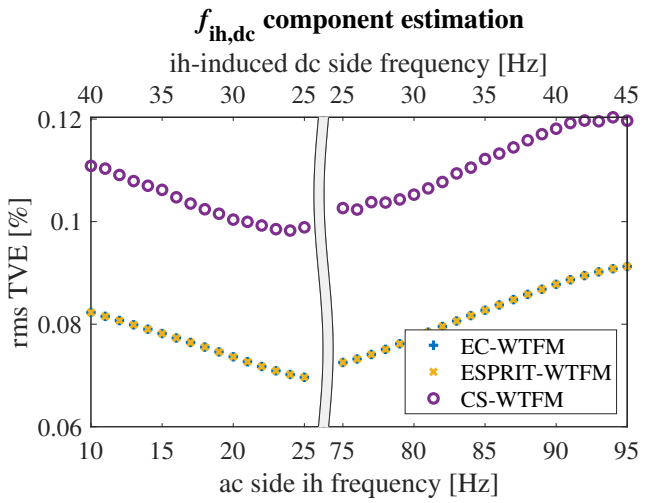

Fig. 7: Interharmonic test (SNR 80 dB) – rms TVE of the $f_{\text{ih,dc}}$ component estimation.

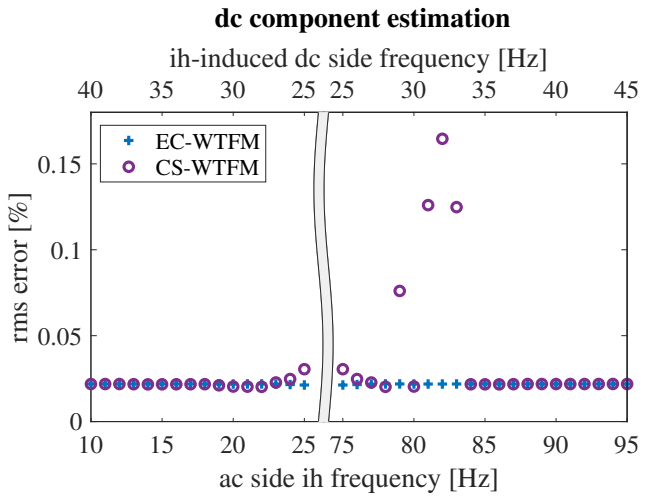

Fig. 8: AM + interharmonic test (SNR 80 dB) – rms error of the dc component estimation. Values for ESPRIT-WTFM (not reported in the figure) are around 7.6 % for each considered inter-harmonic frequency.

each ac component, when relevant, has been considered as produced by a combination of AM and PM effects whose modulation indexes (k_x and k_a, respectively, as in [29]) allow matching the behavior observed in the numerical simulation of the rectifier.

All the tests of Section V-A have been repeated in the presence of 10 % AM with $f_m = 5$ Hz modulation frequency and some exemplary results are reported in Figs. 8 and 9 for dc and interharmonic component estimation, respectively.

The first critical difference with respect to previous results is that ESPRIT-WTFM fails to deal with AM conditions. Indeed, ESPRIT inherently splits the central and sideband components induced by the sinusoidal modulation, thus leading to two different WTFM models whether the proposed clustering approach is applied or not. ESPRIT-WTFM considers all the spectral lines as standalone, and models them with first order expansions: this results in a significant model mismatch for

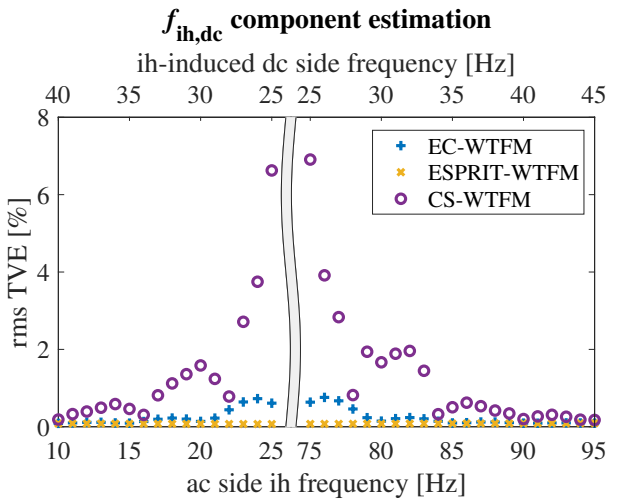

Fig. 9: AM + interharmonic test (SNR 80 dB) – rms TVE of the $f_{\text{ih,dc}}$ component estimation.

all the dynamic components. In particular, as far as dc is concerned, ESPRIT-WTFM separates the dc stationary contribution (0 Hz frequency) from its dynamics that are located at 5 Hz in this case. The estimation error corresponds thus to the fluctuation itself, which is misinterpreted as a single low-frequency component, thus making ESPRIT-WTFM completely unreliable under these conditions. For this very reason, ESPRIT-WTFM results are not reported in Fig. 8, where the advantages of EC-WTFM become instead evident. EC-WTFM and CS-WTFM are both able to capture the dynamics of the dc thanks to the fourth order Taylor expansion, but, in the presence of specific interharmonics and noise, CS-WTFM shows higher rms errors. Such slight degradation is due to occasional errors in the support reconstruction. For instance, when $f_{\text{ih,ac}} = 82$ Hz, a 16 Hz component is rarely found and the resulting TFM model is less effective in tracking dc changes.

Also for ac time-varying components (e.g., the modulated 600 Hz), ESPRIT-WTFM cannot follow accurately their dynamics, while the other methods behave almost the same (in the worst case rms TVE is 0.75 % or 0.74 % for EC-WTFM and CS-WTFM, respectively).

When the steady-state components are considered instead, the responses of the algorithms are different as it can be seen in Fig. 9, which reports the TVE values from the estimation of the lowest frequency dc-side component induced by the interharmonic. Here ESPRIT-WTFM results are reported just to stress again the specificity of the method, i.e., the side effect of the absence of any clustering. The interharmonic is well represented through a first order expansion and ESPRIT provides a good initial estimate of its frequency. ESPRIT-WTFM accurately finds all the tones, thus it results in their almost ideal cancellation while extracting the component having frequency $f_{\text{ih,dc}}$. Under these conditions it performs even better than EC-WTFM, which instead approximately cancels a broader band around the estimated central frequency of each dynamic component. This apparently paradoxical behavior is however the result of lucky circumstances. In fact, interfering

components to be rejected exhibit purely sinusoidal modulations and thus they correspond to the superposition of few isolated stationary tones: this perfectly matches the underlying model of ESPRIT-WTFM.

On the other hand, CS-WTFM results, as in the static scenarios, are influenced by the infiltration of noise but, in this case, the presence of modulation and interharmonic on the ac side produces a complex dc-side waveform, made of many components. As mentioned above, the greedy CS algorithm is not always able to reach the optimal support (even considering the discrete frequency grid), resulting in significant TVE values in some cases. EC-ESPRIT is instead able to always recover correctly the support of the multitone signal and, although errors increase as a lower interharmonic frequency component appears at the dc side, the rms TVE values are always below $1\,\%$.

C. Discussion on Computational Load

The three methods considered during the tests use the same WTFM approach as a second stage, thus they differ only in terms of spectral support retrieval. Finding a different number of frequencies (CS-WTFM with respect to ESPRIT-based methods) or adopting clustering (EC-WTFM with respect to ESPRIT-WTFM) may result in a different computational load, thus it is better to start with the analysis of the complexity of a single component estimation.

The common stage, i.e., WTFM estimation corresponds to the application of two complex filters to extract the synchrophasor and its first derivative, the latter required by for frequency estimation. However, the coefficients of such filters need to be computed. In practice, this corresponds to computing $\mathbf{B}_w$ and then solving (6). The first step results in $2 \cdot N_w \cdot N_p$ multiplications, where $N_p = \sum_{q=0}^{Q}(2K_q+2)$ is the number of parameters in $\bar{\mathbf{p}}$, since $\mathbf{B}$ is $N_w \times N_p$. As an example, under steady-state conditions (the simplest one), $N_p = 20$, 12 and 6 for CS-WTFM, EC-WTFM and ESPRIT-WTFM, respectively, and it varies based on the different choices for expansion orders[3]. The computational burden of the second step depends on the LS solution, which can be performed, for instance, via QR decomposition. If Householder QR decomposition is used and $N_p \ll N_w$ (as it is always the case in our tests), the main contribution to the number of floating point operations (flops) is proportional to $N_p^2 N_w$, thus $\mathcal{O}(N_w)$ considering only the dependency on the number of samples in a real implementation. The LS solution requires then an orthogonal matrix multiplication and backwards substitution, which are lighter.

The main difference between the considered algorithms is in the computational burden of support recovery. CS-WTFM uses an iterative approach and thus the number of flops depends significantly on the waveform spectral content. In the tests, the $Q_{\max}$ components are always considered and the CS search procedure involves, at each ith iteration, $2D_i \cdot N_w$ multiplications, where D_i is the cardinality of the frequency candidates set and can thus be in the order of thousands (if no constraints are added). Then a LS solution with the partial frequency support (that grows with i) and residual energy computation are required. On the other end, the computational burden of frequency support computation is almost the same for EC-WTFM and ESPRIT-WTFM, because they are both based on the same ESPRIT estimation, while clustering has a negligible impact. ESPRIT mainly requires the autocorrelation matrix computation (which depends on M and L, but can be considered as $\mathcal{O}(N_w^3)$ in our tests), the SVD computation ($\mathcal{O}(M^3)$) to find P, $\mathbf{U}$, the LS solution corresponding to (19) (again the main contribution to the number of flops is proportional to $(2P+1)^2 \cdot (M-1)$), the computation of the eigenvalues of $\hat{\hat{\mathbf{\Psi}}}$ (which depends on P^3) and frequencies computation (which is negligible). A full discussion of the exact number of flops is beyond the scope of this paper and strongly depends on the peculiar implementation of each step, but, from the above considerations, a complexity of $\mathcal{O}(N_w^3)$ can be assumed for ESPRIT-based methods.

To verify the feasibility of the proposed methods, the average execution times have been evaluated using a MATLAB implementation of the methods in a PC equipped with Intel(R)-Core(TM) i7-11900 CPU at $2.50\,$GHz. It is important to highlight that no code parallelization nor optimization has been introduced. Different results have been found in terms of execution time for the two classes of methods considered. The CS-WTFM method takes a variable time depending on the spectral content of the analyzed signal, i.e., from about 30 ms for the simplest case (stationary) up to about 80 ms for the tests with a richer spectrum to be recovered. The ESPRIT-based methods, instead, have required about 30 ms, abstracting from the considered test. A real-time implementation of the algorithms is beyond the scope of the paper, but these preliminary results prove that EC-WTFM can guarantee a RR of at least 30-32 measurements per second without any *ad hoc* optimization, whereas CS-WTFM has run at more than 12 (up to 34 under nominal conditions) measurements per second, but its execution time, as already discussed, is not constant. Such results are promising in view of a real implementation on dedicated hardware, since achieving tens of real-time measurements per second appears to be a reasonable target.

VI. Conclusion

The paper has discussed the introduction of synchronized measurements and dedicated algorithms to monitor and track PQ in dc grids. The importance of adopting advanced measurement techniques, such as those based on TFM models, was demonstrated to effectively cope with multitone and dynamic waveforms. The performance unlocked thanks to TFM models is tied to a proper detection of the spectral support of the analyzed signals. Two viable approaches have been analyzed and compared.

The first, CS-WTFM, is based on a greedy CS-based algorithm, relying on a discrete frequency grid. The second, EC-WTFM, relies on the ESPRIT technique, which the authors have properly modified and combined with a clustering method in order to operate also in the presence of modulated components. Simulation results show that both CS-WTFM

[3]No clusters are needed in this case.

and EC-WTFM algorithms enable remarkable accuracy in estimating dc and ac components. It is worth noting that generally EC-WTFM leads to slightly better results, while the performance of CS-WTFM depends on its settings, which enable retrieving the correct support cardinality. On the other hand, the straightforward application of ESPRIT for support recovery (ESPRIT-WTFM) may lead to gross errors in the presence of dynamics.

As a final consideration, synchronization in dc measurements revolutionizes the paradigm because disturbance characterization through concise energy or statistical parameters is not the only possibility, and synchronized measurements can also help in improving indexes evaluation. Such new measurements can be regarded as a possible first step towards coordinated monitoring. New applications can emerge on wider and more heterogeneous networks. Just to mention an example, it would be possible to integrate ac and dc synchronized measurements to have a better picture of the status also in hybrid ac/dc networks. Another possibility could be analyzing the propagation of the dc ripple, which relies on the capability to accurately measure in a synchronized way instantaneous frequency and phasors of the ac components at a grid level.

REFERENCES

[1] B. Mohandes, M. S. E. Moursi, N. Hatziargyriou, and S. E. Khatib, "A review of power system flexibility with high penetration of renewables," *IEEE Transactions on Power Systems*, vol. 34, no. 4, pp. 3140–3155, 2019.

[2] F. Nejabatkhah and Y. W. Li, "Overview of power management strategies of hybrid ac/dc microgrid," *IEEE Transactions on Power Electronics*, vol. 30, no. 12, pp. 7072–7089, 2015.

[3] J. Yu, K. Smith, M. Urizarbarrena, N. MacLeod, R. Bryans, and A. Moon, "Initial designs for the ANGLE dc project; converting existing ac cable and overhead line into dc operation," in *13th IET International Conference on AC and DC Power Transmission (ACDC 2017)*, 2017, pp. 1–6.

[4] A. Clerici, R. Chiumeo, and C. Gandolfi, "MVDC multi-terminal grids: a valid support for distribution grids improvement," in *2020 AEIT International Annual Conference*, 2020, pp. 1–6.

[5] Z. Yang, H. Zhong, A. Bose, Q. Xia, and C. Kang, "Optimal power flow in ac–dc grids with discrete control devices," *IEEE Transactions on Power Systems*, vol. 33, no. 2, pp. 1461–1472, 2018.

[6] A. Dognini, M. Ginocchi, E. De Din, F. Ponci, and A. Monti, "Service restoration of ac–dc distribution grids based on multiple-criteria decision analysis," *IEEE Access*, vol. 11, pp. 15 725–15 749, 2023.

[7] M. H. J. Bollen, R. Das, S. Djokic, P. Ciufo, J. Meyer, S. K. Rönnberg, and F. Zavodam, "Power quality concerns in implementing smart distribution-grid applications," *IEEE Transactions on Smart Grid*, vol. 8, no. 1, pp. 391–399, 2017.

[8] *European Committee for Electrotechnical Standardization Voltage Characteristics of Electricity Supplied by Public Electricity Networks*, EN 50160:2016, Dec 2016.

[9] *IEC Electromagnetic compatibility (EMC) - Part 4-30: Testing and measurement techniques - Power quality measurement methods*, IEC 61000-4-30:2015, Dec. 2015.

[10] *IEC Electromagnetic compatibility (EMC) Part 4-7: Testing and measurement techniques - General guide on harmonics and interharmonics measurements and instrumentation, for power supply systems and equipment connected thereto*, IEC 61000-4-7/A1:2008, Jun. 2008.

[11] A. A. Alkahtani, S. T. Y. Alfalahi, A. A. Athamneh, A. Q. Al-Shetwi, M. B. Mansor, M. A. Hannan, and V. G. Agelidis, "Power quality in microgrids including supraharmonics: Issues, standards, and mitigations," *IEEE Access*, vol. 8, pp. 127 104–127 122, 2020.

[12] A. Mariscotti, "Power quality phenomena, standards, and proposed metrics for dc grids," *Energies*, vol. 14, no. 20, 2021. [Online]. Available: https://www.mdpi.com/1996-1073/14/20/6453

[13] D. Signorino, A. D. Femine, D. Gallo, E. G. Armando, J. J. Melero Estela, J. J. Pérez-Aragüés, and D. Giordano, "Analysis of ac oscillations in a dc smart grid," in *2024 IEEE 14th International Workshop on Applied Measurements for Power Systems (AMPS)*, 2024, pp. 1–6.

[14] G. Cipolletta, A. D. Femine, D. Gallo, Y. Seferi, F. Fan, and B. G. Stewart, "Detection of dips, swells and interruptions in dc power network," in *2022 20th International Conference on Harmonics & Quality of Power (ICHQP)*, 2022, pp. 1–6.

[15] J. Barros, M. De Apráiz, and R. I. Diego, "Definition and measurement of power quality indices in low voltage dc networks," in *2018 IEEE 9th International Workshop on Applied Measurements for Power Systems (AMPS)*, 2018, pp. 1–5.

[16] G. Frigo and F. Costa, "Dc power metering in low-voltage microgrids: Definitional and methodological issues," in *2023 4th International Conference on Smart Grid Metrology (SMAGRIMET)*, 2023, pp. 1–6.

[17] M. C. Magro, A. Mariscotti, and P. Pinceti, "Definition of power quality indices for dc low voltage distribution networks," in *2006 IEEE Instrumentation and Measurement Technology Conference Proceedings*, 2006, pp. 1885–1888.

[18] I. Ciornei, M. Albu, M. Sanduleac, L. Hadjidemetriou, and E. Kyriakides, "Analytical derivation of PQ indicators compatible with control strategies for dc microgrids," in *2017 IEEE Manchester PowerTech*, 2017, pp. 1–6.

[19] A. Delle Femine, D. Gallo, C. Landi, M. Luiso, H. E. van den Brom, and R. van Leeuwen, "Assessment of quasi-stationary power quality phenomena in dc power systems," *Measurement*, vol. 242, p. 115844, Jan. 2025.

[20] *IEC TR 63282 - LVDC systems - Assessment of standard voltages and power quality requirements ED2"*, IEC TR 63282:2020, Dec 2015.

[21] G. Frigo, R. Van Leeuwen, H. Van Den Brom, D. Signorino, D. Giordano, D. Gallo, and A. D. Femine, "Inter-laboratory comparison of reference systems for dc power quality measurements," in *2024 IEEE 14th International Workshop on Applied Measurements for Power Systems (AMPS)*, 2024, pp. 1–6.

[22] M. Zanoni, R. Chiumeo, L. Tenti, C. Laurano, S. Toscani, and P. A. Pegoraro, "Synchronized measurements for monitoring power quality in dc systems: A proposal," in *2023 IEEE 13th International Workshop on Applied Measurements for Power Systems (AMPS)*, 2023, pp. 1–6.

[23] M. Bertocco, G. Frigo, C. Narduzzi, C. Muscas, and P. A. Pegoraro, "Compressive sensing of a Taylor-Fourier multifrequency model for synchrophasor estimation," *IEEE Transactions on Instrumentation and Measurement*, vol. 64, no. 12, pp. 3274–3283, 2015.

[24] G. Frigo, P. A. Pegoraro, and S. Toscani, "Enhanced support recovery for PMU measurements based on Taylor–Fourier compressive sensing approach," *IEEE Transactions on Instrumentation and Measurement*, vol. 71, pp. 1–11, 2022.

[25] R. Roy, A. Paulraj, and T. Kailath, "ESPRIT–a subspace rotation approach to estimation of parameters of cisoids in noise," *IEEE Transactions on Acoustics, Speech, and Signal Processing*, vol. 34, no. 5, pp. 1340–1342, 1986.

[26] X. Shan, D. Macii, D. Petri, and H. Wen, "Enhanced IpD2FT-based synchrophasor estimation for M class PMUs through adaptive narrowband interferers detection and compensation," *IEEE Transactions on Instrumentation and Measurement*, vol. 73, pp. 1–14, 2024.

[27] J. A. de la O Serna, "Dynamic phasor estimates for power system oscillations," *IEEE Transactions on Instrumentation and Measurement*, vol. 56, no. 5, pp. 1648–1657, Oct. 2007.

[28] M. H. Hayes, *Statistical Digital Signal Processing and Modeling*. New York: John Wiley & Sons, 1996.

[29] *IEEE/IEC International Standard - Measuring relays and protection equipment - Part 118-1: Synchrophasor for power systems - Measurements*, IEC/IEEE 60255-118-1, Dec 2018.

Riccardo Chiumeo received the M.Sc. (*cum laude*) in electrotechnical engineering from Politecnico di Milano. During his working career, which began in ENEL Ricerca, he gained experience in the field of quality of electrical supply and power electronics. He was responsible for activities related to monitoring and improving, through innovative devices, the quality of voltage in MV and LV distribution networks, the meshing of the MV distribution network through DC connections and the protection of distribution networks issues in the field of the Research Fund for the Italian Electrical System. He is currently the head of the Technologies for Active Distribution Networks research group, Transmission and Distribution Technologies Departement, Ricerca sul Sistema Energetico S.p.A, Milan. He is member of the CEI (Italian Electrotechnical Committee) CT 8/123 technical committee (Systems aspects for electrical energy supply) and vice-president of SC 210/77A subcommittee (Low-frequency phenomena).

Christian Laurano (Member, IEEE) received the M.S. and Ph.D. degrees *cum laude* in electrical engineering from the Politecnico di Milano, Milan, Italy, in 2014 and 2018, respectively. From 2021 to 2024 he was an Assistant Professor with the Dipartimento di Elettronica, Informazione e Bioingegneria, Politecnico di Milano, where he is currently Associate Professor. His main research interests include innovative methods to model and characterize electrical transducers, devices and components, diagnostic techniques devoted to electrical grid components, and power quality monitoring.

Paolo Attilio Pegoraro (Senior Member, IEEE) received the M.Sc. (*summa cum laude*) degree in telecommunication engineering and the Ph.D. degree in electronic and telecommunication engineering from the University of Padova, Padua, Italy, in 2001 and 2005, respectively. From 2015 to 2018 he was an Assistant Professor with the Department of Electrical and Electronic Engineering, University of Cagliari, Cagliari, Italy, where he is currently Associate Professor.

He has authored or co-authored over 180 scientific papers. His current research interests include the design of new measurement techniques for power networks, with attention to synchronized measurements and state estimation.

Dr. Pegoraro is a member of IEEE IMS TC 39 (Measurements in Power Systems) and of IEC TC 38/WG 47. He is also a member of IEEE EPPC WG on Energy. He is an Associate Editor in Chief of the IEEE Transactions on Instrumentation and Measurement and the General Chair of the IEEE International Workshop on Applied Measurements for Power Systems (AMPS).

Antonio Vincenzo Solinas (Member, IEEE) received the M.S. degree in Electronic Engineering and the Ph.D. degree in industrial engineering from University of Cagliari, Italy, in 2000 and 2022, respectively. He worked for almost twenty years as an R&D manager on audio and video acquisition, compression and transmission over IP.

He is currently an Assistant Professor with the Electrical and Electronic Measurements Group, Department of Electrical and Electronic Engineering, University of Cagliari. He has co-authored about twenty scientific articles published in international journals and conference proceedings. His main research interests include optimization techniques for estimation and monitoring in power systems with attention to synchronized measurements. He is member of the IEEE Instrumentation and Measurement Society.

Liliana Tenti is a Senior Scientist at RSE -Ricerca sul Sistema Energetico, Italy. She receives her degree in Solid State Physics from the University "La Statale" of Milan, Italy. Her main research interests are in power distribution systems with a focus on Power Quality analysis and Artificial Intelligence techniques applied to data from voltage monitoring systems. She is currently an IEEE PES and AEIT member and secretary of SC 210/77A subcommittee (Low-frequency phenomena).

Sergio Toscani (Senior Member, IEEE) received the M.S. (*summa cum laude*) and the Ph.D (*summa cum laude*) degrees in electrical engineering from the Politecnico di Milano, Italy, in 2007 and 2011, respectively.

From 2011 to 2020 he was Assistant Professor in Electrical and Electronic Measurement with the Dipartimento di Elettronica, Informazione e Bioingegneria, Politecnico di Milano, where he currently serves as an Associate Professor. His research activity is mainly focused on development and testing of current and voltage transducers, measurement techniques for power systems, electrical components and systems diagnostics. He is member of the IEEE Instrumentation and Measurement Society, of the IEEE TC-39 - Measurements in Power Systems and Technical Program Co-Chair of the IEEE International Workshop on Applied Measurements for Power Systems (AMPS).

Michele Zanoni (Member, IEEE) was born in Codogno, Italy, in 1991. He received the M.Sc. (*cum laude*) and the Ph.D. degrees in electrical engineering from the Politecnico di Milano, Milan, Italy, in 2015 and 2019, respectively.

From 2018 to 2019, he was PostDoc researcher at the Dipartimento di Elettronica, Informazione e Bioingegneria at Politecnico di Milano where his research activities were focused on development of innovative approaches to the modeling and identification of frequency-domain nonlinear systems devoted to the characterization of power system transducers and components. From 2020 he holds a permanent research position at Technologies for Active Distribution Networks research group, Transmission and Distribution Technologies Departement, Ricerca sul Sistema Energetico S.p.A, Milan. His current research interests include power quality measurements and algorithms for distributed monitoring system in power system application and modeling of high-frequency disturbances. He is Member of the IEEE, Member of the CEI (Italian Electrotechnical Committee) CT 8/123 technical committee and the IEC TC 8/JWG 9 working group.